QUASI-STATIC AND DYNAMIC THORACIC LOADING TESTS: CADAVERIC TORSOS

Greg Shaw, David Lessley, Jay Evans, Jeff Crandall, Jaeho Shin
University of Virginia Center For Applied Biomechanics

Pascal Portier
CEESAR

Gabriele Paoloni
Vicon UK

ABSTRACT

This NHTSA-sponsored study evaluated the response of five male cadaver torsos to quasi-static and dynamic anterior loading by rigid rectangular indentors designed to approximate a section of a shoulder belt. Indentor load and three-dimensional deflection measurements were recorded in order to quantify regional force-deflection and mechanical coupling of the anterior ribcage. Fractures were identified by post test necropsy. Dynamic loading produced higher forces than did quasi-static loading and the sternum was found to be stiffer than either the upper or lower loading ribcage sites for which similar stiffnesses were recorded. Rib fractures, many of which occurred at the costa-chondral junction, did not necessarily reduce the ability of the chest to resist anterior loading. The effects of rib fracture are most evident when loading the lower lateral rib cage and when there are many bicortical fractures. Bicortical fractures were more common for the older subjects whose ribcage cartilage was more calcified. The patterns of mechanical coupling were similar for different subjects, test conditions, and indentor compression levels. In most cases, the deflection toward the spine was greater than the lateral and inferior movement at any measurement site. In general, both the stiffness results and coupling patterns found in this study were similar to those previously reported for a prior benchmark study that used comparable methods. This study yields information required to develop computational and physical thorax models that exhibit improved biofidelic loading response.

Keywords: Ribcage, force-deflection, coupling, cadavers, rib fractures

INJURY TO THE CHEST is the principle cause of death in approximately 30 percent of traffic fatalities (Mulligan et al., 1994). Since the early 1960s, the goal of reducing chest injuries has motivated numerous studies of human thoracic response to loading conducted (Backaitis, 1994). Thoracic deformation due to anterior chest loading is generally accepted as the parameter that best correlates to rib and sternal fractures, the most frequently observed thoracic injury for occupants in vehicles equipped with contemporary restraint systems (Kent et al., 2003b).

Improved biofidelity of the chest subjected to restraint loading remains a priority for improving frontal impact dummies. A simulated impact (sled test) provides the most realistic conditions for defining human response (as approximated by cadavers, the best available human surrogate) and, therefore, for assessing dummy chest biofidelity. However, this environment compromises the ability to isolate and measure thoracic response accurately. Knowing how the human body responds on a regional and sub-regional level facilitates the design of dummy components and sub-systems such as the ribs and ribcage. Components that demonstrate approximate human response is the necessary first step in the construction of a dummy designed to respond biofidelically in a simulated crash.

Several test series designed to study the effects of regional quasi-static anterior loading on cadavers and the Hybrid III and THOR prototype frontal impact dummies were conducted at Wayne State University Bioengineering Center and at the University of Michigan Transportation Research Institute (UMTRI) (Cavanaugh et al., 1988, Schneider et al., 1989, 1992b). The Cavanaugh tests were designed to measure the extent that ribs adjacent to the loading site moved (i.e., coupling effects) and the

regional stiffness at locations where belt load would be applied to the torso (Figure 1). For these tests, the magnitude of coupling was expressed as the relative deflection response of sites remote to the site that was deflected 25.4 mm downward by a gimbaled rectangular indentor.

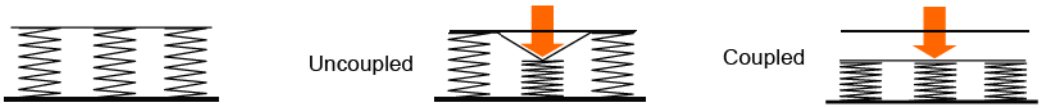

Figure 1. Coupling illustrated.

When these tests were reproduced at the University of Virginia (UVA) by Shaw et al. (2005) using the Hybrid III and the THOR Alpha frontal crash dummies, the dummy responses differed from cadaver subjects in terms of coupling and stiffness. This study uses a methodology similar to that employed by Cavanaugh but adds conditions and instrumentation that yield additional information required to develop computational and physical thorax models that exhibit improved biofidelic loading response. In addition to quasi-static loading, the subjects were loaded dynamically at a rate similar to that experienced during restraint belt loading in a frontal crash. Whereas the Cavanaugh tests measured X-axis (sternum-to-spine) deflection, these tests recorded three-dimensional (3-D) movement of points on the anterior ribcage not under the indentor. While X-axis chest deflection has been studied extensively (Yoganandan et al., 1991, Kroell, 1994, Kuppa and Eppinger, 1998), lateral and vertical ribcage motion has been observed in response to anterior loading of human cadavers (Yoganandan et al., 1991, Crandall et al., 1997, Shaw et al., 2004). Although the significance of ribcage deflection in directions other than sternum-to-spine with respect to injury has not been established, accurate three-dimensional motion is required to construct a biofidelic surrogate thorax.

METHOD

This study evaluated the response of five male cadaver torsos to anterior loading provided by rigid rectangular indentors that approximated a segment of a shoulder belt (Figure 2). Three sites that coincided with the path of a shoulder belt restraint were loaded quasi-statically and dynamically (1.0 m/s) with an indentor mounted to a load cell. Triaxial deflection measurements were taken at eight to nine measurement locations. Fractures were identified by post test necropsy. Table 1 summarizes the test parameters and components.

SUBJECTS: Five male cadavers (Table 2) that met the following criteria were selected for the study:

1) Free of HIV and hepatitis B and C
2) Structurally intact rib cages (as determined by CT)
3) Weight and chest depth similar to the 50th percentile male
4) Preserved by refrigeration / freezing (not embalmed)

The subjects were prepared by first removing the head and extremities. Skin and soft tissue were removed from the anterior and lateral aspects of the torso. A perforated steel plate was screwed to the spine and pelvis. Wood screws were placed bilaterally through 10 vertebrae from T1 to L5 and the posterior iliac crests. The torso with attached plate was mounted on a 19 mm thick plywood platen. The process of securing the spine to a planar structure eliminated all or most of the spinal curvature in the sagittal plane and prevented any lateral or superior/inferior movement of the torso. Because the screw heads were supported by the plywood, the vertebrae in which they were installed could not move posteriorly in response to indentor loading on the anterior rib cage. However, the posterior ribs were not rigidly fixed and could move toward the platen as much as the overlying skin and soft tissue, compressed by the process of screwing the vertebrae, would allow. Subject preparation concluded by marking indentor sites and attaching Vicon retro-reflective markers and strain gages as described below.

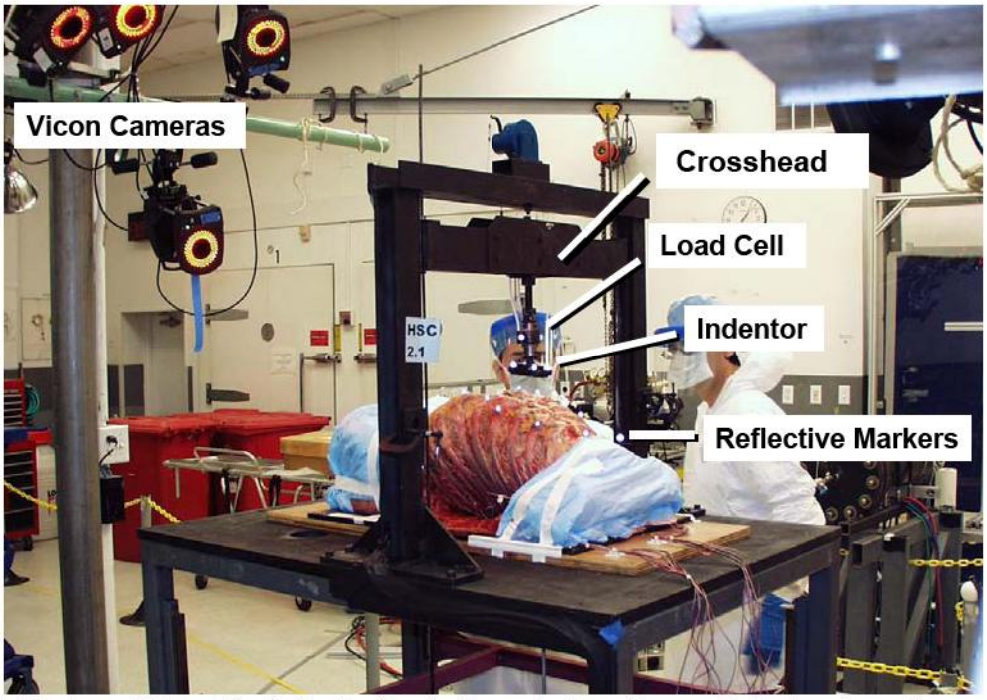

Figure 2. Test condition. The indentor loads the anterior ribcage. Indentor force is recorded by the load cell.

Table 1. Test Parameters, Hardware, and Instrumentation

Item	Description / Specifications	Comment
Loading Device	Instron materials test machine	The Instron was used to power a remote crosshead via hydraulic cylinders.
Indentors	Rectangular aluminum contact plates. Overall dimensions 62 x 113 mm and 62 x 62 mm.	A ball joint above the indentor contact plate allows ~15 degrees of indentor rotation allowing some conformation to local chest contours.
Indentor Velocity	Quasi-static: 1.7 mm/s Dynamic: 1000 mm/s (1.0 m/s)	
Indentor Stroke	Pre condition sinusoidal: 12 mm Non-injurious: 18 - 30 mm Injurious: 80 mm	Non-injurious test indentor stroke adjusted to subject chest depth. Dynamic test peak deflections typically overshot target.
Indentor Preload	25 $\pm$ 5 N.	The indentor preload allowed the indentor to align itself with the rib cage contours.
Indentor Loading Sites	The center of the indentor face was aligned with three sites on the anterior chest (Figures 3 and 4).	The upper site was left rib 3 and the lower site was right rib 6 for subjects 1-4. Sides were reversed for subject 5 because left rib 2 was not joined to the sternum.
External Deflection Measurement Sites	10 sites: 3 indentor sites (Figures 3 and 4).	The Vicon camera system recorded triaxial displacement of spherical markers glued to the ribcage at those sites not covered by the indentor. The loaded site uniaxial (X-axis) deflection was assumed to be the movement of the remote crosshead as measured by a string potentiometer.
External Force Measurement	A six-axis load cell above the indentor recorded force applied by the subject on the indentor (Figure 2).	Time histories were recorded for indentor force data. Only the force parallel to the path of the indentor stroke (X-axis) was used for analysis.
Subjects	Five male cadaver torsos. Skin and soft tissue was removed from anterior and lateral aspects.	Prior to removal of the head, extremities, and torso soft tissue, the subject masses were similar to the 50th percentile male. See Tables 2 and 4.
Subject Support	The subject spines were screwed to a 19 mm thick plywood platen via a perforated steel plate. Wood screws were placed bilaterally through 10 vertebrae from T1 to L5 and the posterior iliac crests (Figure 2).	The process of screwing the spine to a planar structure eliminated all or most of the spinal curvature and its effect on the force-deflection response. This process also prevented any lateral or superior/inferior movement of the torso.

Table 2. Subject Summary Table

	1	2	3	4	5
Number	343	342	320	319	203
Age at Death	72	75	48	52	67
Cause of Death	End stage liver disease	End stage Parkinson's disease	Sudden death	Metastatic renal cell cancer	Metastatic Cancer
Rib Cage Observations [A]	Costal cartilage calcified bilaterally at the level of the 6th and 7th ribs.	Cartilage beginning to deteriorate at time of autopsy.	Pliable cartilage.	Very pliable cartilage.	Calcification of cartilage is variable. Cartilage of right rib 5 most calcified. Left rib 2 costal cartilage is absent: the rib does not join the sternum.
Rib Cage Bone Condition [B]	Moderate	Moderate to Severe	Mild	Moderate	None
Height (cm)	180	183	168	179	170
Weight (kg) [C]	66	73	68	77	77
Chest Depth [C] (average at level of lateral aspect of ribs 4 and 8) (cm)	22.3	21.9	17.5	18.5	20.8

Notes:
A – Determined after removal of superficial soft tissue.
B – Qualitative bone condition determined by radiologist from CT images.
C – Prior to the surgical removal of anterior and lateral torso skin and soft tissue, head, and extremities.

LOADING DEVICE: All tests began with the subject torso supine under the rigid planar indentor. A computer-controlled Instron material testing machine was used to provide the anterior-posterior deflection via a remote hydraulically actuated crosshead (Figure 2). The indentor was mounted under the crosshead. Indentors with contact plates measuring 62 x 113 mm (2x4") and 62 x 62 mm (2x2") were tested. Three millimeter thick natural rubber pads were added to the plates in order to reduce edge stress concentrations on the denuded rib cage. The rubber contact areas measured 58 x 105 mm and 58 x 58 mm. The contact area of the indentor was intended to simulate a section of a shoulder belt.

ANTERIOR TORSO LOADING SITES: The center of the indentor face was aligned with three sites on the anterior chest including the sternum at rib 5 (S5), the left side on rib 3 (L3) at costo-chondral (CC) junction, and the right side at rib 6 (R6) at CC junction (Figures 3 and 4). Note that the sides were reversed for subject 5 because left rib 2 was not joined to the sternum (discovered after soft tissue removal). The calculation of averages required the assumption of response symmetry for subject 5 data. For most of the tests, the indentor was rotated 30 degrees with respect to the sternum centerline to approximate the orientation of a shoulder belt segment.

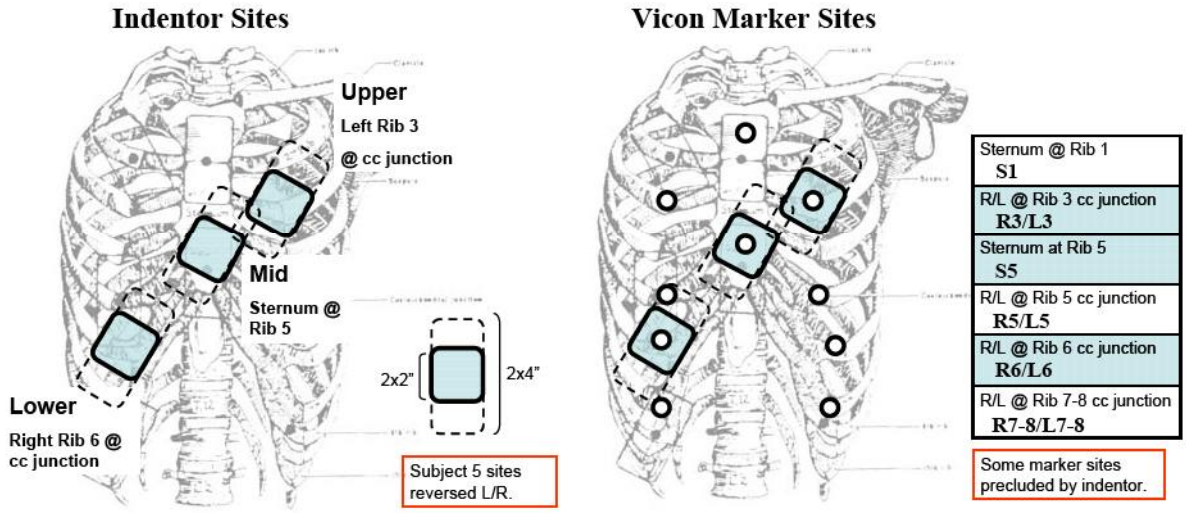

Figure 3. Indentor and marker sites. Most tests were conducted with the 2x2" indentor. Shaded squares indicate loading sites. Marker sites are indicated by circles.

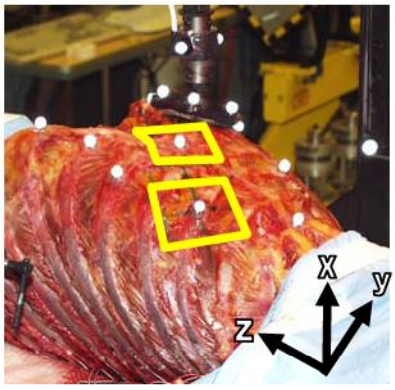

Figure 4. Marker and loading site locations (shown here at pre test for loading (R6). Marker sites are indicated by spherical reflective markers on the anterior thorax. Two of the three loading sites are indicated by box-shaped yellow perimeters representing the indentor target. Negative X is toward the spine, positive Y toward the right, and positive Z toward the pelvis.

MEASUREMENTS, INSTRUMENTATION, AND DATA ACQUISITION: Indentor force was measured by a multi-axis load cell mounted between the crosshead and the indentor. Indentor/crosshead deflection along the X-axis (sternum to spine) was measured by a string potentiometer and by an array of eight Vicon MX13 cameras (Figure 2) that also recorded the three axis motion of the rib and sternal sites. Spherical reflective markers were placed on the site bone surface (Figures 3 and 4).

The string potentiometer and load cell data were acquired at 10,000 samples per second for the dynamic tests and at 200 samples per second for the quasi-static tests. Vicon data was collected at 1000 samples per second for the dynamic tests and at 50 samples per second for the quasi-static tests.

TEST MATRIX: Subject 1 tests varied somewhat from the subject 2 - 5 tests (Tables 3 and 4). Subject 1 tests included varying indentor size and orientation but did not include quasi-static tests at low, non-injurious deflection levels. All subjects were "preconditioned" by deflecting the mid sternum with 10 one second sinusoidal deflections with a 12 mm peak. This non-injurious loading was intended to obtain a consistent force-deflection response from each subject (Kent et al., 2004).

Table 3. Subject 1 Test Matrix

Test	Indentor [A]	Site [B]	Deflection [C]	
			Low [D]	To Failure [E]
1.2	2x4	Mid	x	
1.3	2x2	Mid	x	
1.4	2x2	Upper	x	
1.5	2x4	Upper	x	
1.6	2x4	Lower	x	
1.7	2x2	Lower	x	
1.8	2x4 -15 deg	Lower	x	
1.9	2x4 +15 deg	Lower	x	
1.12	2x4	Lower		x

Notes:
A - Indentors: 62 x 113 mm (2x4") and 62 x 62 mm (2x2"). Indentors oriented 30 from vertical with respect to the long axis of the torso with the exception of tests 1.8 and 1.9.
B - Indentor sites: Mid - mid sternum at rib 5, Upper - costochondral junction at rib 3, Lower - costochondral junction at rib 6.
C – All subject 1 tests were dynamic loading events conducted at 1 m/s.
D - Low - non-injurious deflection ranging from 18 to 30 mm depending on tests and subject.
E - Approximately 80 mm.

Table 4. Subjects 2-5 Typical Test Matrix

Test	Indentor	Site	Speed		Deflection	
			Quasi-static	Dynamic	Low	To Failure
2	2x2	Mid	x		x	
3	2x2	Mid		x	x	
4	2x2	Lower		x	x	
5	2x2	Lower	x		x	
6	2x2	Upper	x		x	
7	2x2	Upper		x	x	
8	2x4	Upper		x		x

Note: Table above is specific for subject 2. Subject 3-5 matrices differ in test order, but tests conducted are the same.

The first tests for all subjects consisted of non-injurious deflections at all three sites. The peak deflection values were chosen based on Cavanaugh et al. (1988) who showed that a quasi-static deflection of 25.4 mm did not produce rib fractures but that a 50.8 mm deflection did. This finding was confirmed by the success in avoiding palpable rib fractures in the low deflection tests for subjects 1 and 2. In these tests the peak deflection in the dynamic tests was 30 mm, 13 to 14 percent of the original (non-denuded) subject chest depth averaged at the lateral level of the 4th and 8th ribs (Table 5). Our selection of a non-injurious level was also supported by Eckert et al. (2000) who reported that 40 mm deflection was non-injurious in similar tests of denuded thoraces.

Table 5. Deflection Values

Subject	Ave. Chest Depth [A]	Dynamic Test Steady State Deflection [B, C]	Dynamic Test Peak Deflection	Peak Dynamic Deflection /Chest Depth	Quasi-static Test Deflection	Quasi-static Peak Deflection / Chest Depth
	mm	mm	mm		mm	
1	223	23.2	29.7	0.133	Not Done	-------
2	219	23.5	30.3	0.138	25.0	0.114
3	175	18.5	25.0	0.143	18.7	0.107
4	185	18.7	25.1	0.136	18.0	0.097
5	208	21.9	28.4	0.137	20.5	0.099

Notes:
A - Chest depth average of measurements taken at the lateral level of the 4th and 8th ribs prior to removal of skin and soft tissue.
B - Peak and steady state values are representative of all similar tests for that subject.
C - Steady state dynamic deflection values taken after indentor "bounce" subsided, about 200 ms after T_o.

Peak dynamic deflection for subjects 3 - 5 ranged from 25 to 28 mm reflecting reduced chest depth in comparison to subjects 1 and 2. Static deflection values for subjects 2 - 5 were 10 to 11 percent of original subject chest depth and ranged from 18 to 25 mm.

DATA PROCESSING AND PRESENTATION: Force-Deflection Scaling: Due to the variability in subject geometry and inertial properties, the force-deflection values were normalized to the standard anthropometry of the 50th percentile male weighing 75 kg. The normalization procedures of Eppinger et al. (1984) were used to perform the scaling. This procedure assumes that the mass density and modulus of elasticity are constant between test subjects. The scaling variable based on occupant mass (M) in kg relative to the 50th male (75 kg) is shown in equation (1).

$$\lambda = (75 / M_i)^{1/3} \qquad (1)$$

The scaled test parameters, denoted with subscript s, can then be expressed in terms of the initial parameters, denoted with subscript *i*, and the scaling factor (Eq. 2, 3).

Length: $$L_s = \lambda \times L_i \qquad (2)$$

Force: $$F_s = \lambda^2 \times F_i \qquad (3)$$

Because the subjects (prior to head and limb removal) weighed approximately 75 kg, the scale factors did not substantially affect the results. The force-deflection curves are presented both using mass scaling and mass compensation.

Force-Deflection: Force-deflection results are reported using mass scaled force for quasi-static tests, and mass scaled and mass compensated force for dynamic tests. Mass scaled forces are filtered to CFC 1000 while mass scaled and mass compensated forces are filtered to CFC 180. Deflection data is filtered to CFC 1000. All force deflection results reflect only the X-axis indentor force. Y-axis and Z-axis indentor forces were recorded but did not contribute substantially to the resultant force. The average resultant force was six percent higher when calculated with the Y and Z values. The peak magnitude of the Y and Z force values averaged approximately 22 percent of the X value.

Marker Movement: Coupling results are calculated from the Vicon output X-axis trajectory data for each marker. Marker trajectories were reported in the SAE X,Y, and Z occupant coordinate system (Figure 4). Vicon and analogue sensor data were synchronized to share the same t = 0 event based on the initial movement of the indentor-mounted Vicon markers. Because marker centers were mounted (9 mm) above the target site on the surface of the rib or sternum, rotation of the bone creates marker movement interpreted by the Vicon system as translation. In order to estimate the amount of marker movement due to target site translation, it was necessary to bound the bone rotation values. This was done using the finite element human model, H-model (Handbook of Numerical Analysis, 2004). At 30 mm of X-axis indentor displacement, the model indicated that rotation accounted for a range of 1.6 mm to -0.3 mm for Y-axis and Z-axis marker movement.

Coupling Data Presentation: Figure 5 illustrates the presentation of the quantitative coupling results. In the illustrated test the indentor loads (R6). The colored columns indicate the relative position of each site in response to indentor loading. Indentor displacement, always the maximum recorded in these tests, is labeled a "0.0". A site that recorded no deflection would be labeled "1.0". The column label "0.6" for (S5) indicates that this site moved down 0.4 units (1.0 – 0.6). These proportional values were calculated using the absolute differences in site position along the X-axis. Equation 4 is used for the calculation of values illustrated in the presentation of load site deflection:

$$\text{Calculated value} = 1 - (\text{site deflection})/(\text{indentor deflection}) \qquad (4)$$

Missing columns, such as at (R 7-8), indicate a site where no marker data was collected for that test due to a missing marker at that location. In some cases markers were removed for proper indentor placement and in other cases the Vicon system was not able to track certain markers simultaneously with multiple cameras, thus causing a loss of marker data for that site.

Models of three tests to injury, subjects 1, 3, and 4 were created using the H-Model (Handbook of Numerical Analysis, 2004) in order to illustrate the movement of the ribcage (Appendix Figure A-2). The models were employed to provide only qualitative information.

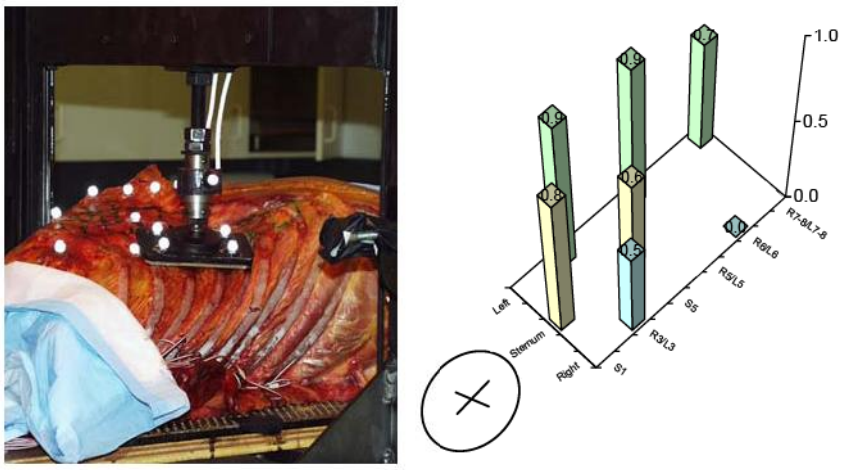

Figure 5. Load site deflection presentation.

Fracture Identification: Fractures were identified during autopsy. The autopsy involved removing the soft tissue over the posterior ribcage in order to allow inspection of the posterior ribs for fracture. None were found for any of the subjects. The lateral and anterior ribcage was then removed from the torso so that the inner surface of ribs could be examined and palpated in order to identify subtle fractures including incomplete (monocortical) or cartilage fractures. The location of the fractures was measured in two ways, an X-Y location relative to the top of the sternum and a distance from the center of the sternum measured along the rib.

RESULTS

The test procedures produced credible data with no mechanical problems and few sensor failures. Marker location data was similarly robust with few instances of markers failing to be visible by a required minimum of two cameras for optical position measurement to be made by the Vicon system.

FORCE-DEFLECTION: Subject force-deflection curves grouped by subject for both the non-injurious quasi-static and dynamic tests are presented in Figure 6. The dynamic response was greater than the quasi-static response, most evident for subjects 3 and 4. Figure 7 presents the five force-deflection curves for the dynamic injurious tests. The sternal loading site for subject 4 produced the highest force (2695N). Figure 8 presents the force-deflection results grouped by indentor site.

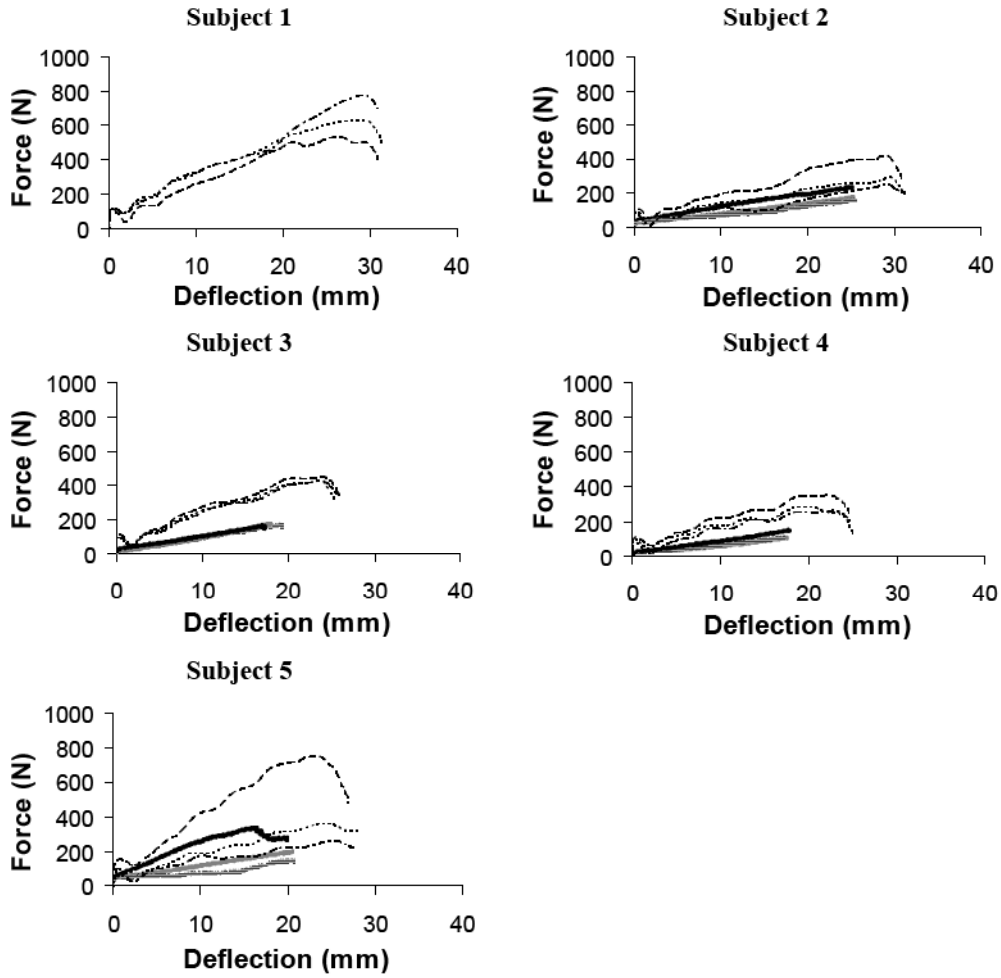

Figure 6. Force-deflection results by subject for quasi-static and dynamic non-injurious tests. Dynamic tests are associated with a slightly greater deflection. Dotted lines are dynamic tests and solid lines are quasi-static tests.

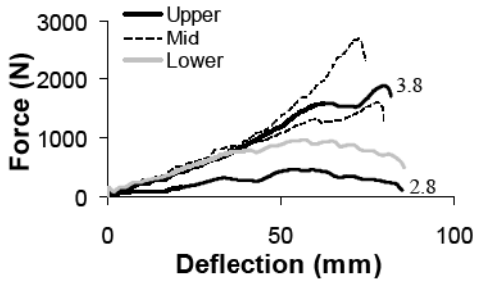

Figure 7. Subject force-deflection curves for injurious dynamic tests. For the two subjects loaded at the lateral 3rd rib (tests 2.8 and 3.8), the injurious test resulted with indentor penetration into the thoracic cavity with a correspondingly reduced force-deflection response. See Figure 17 illustration.

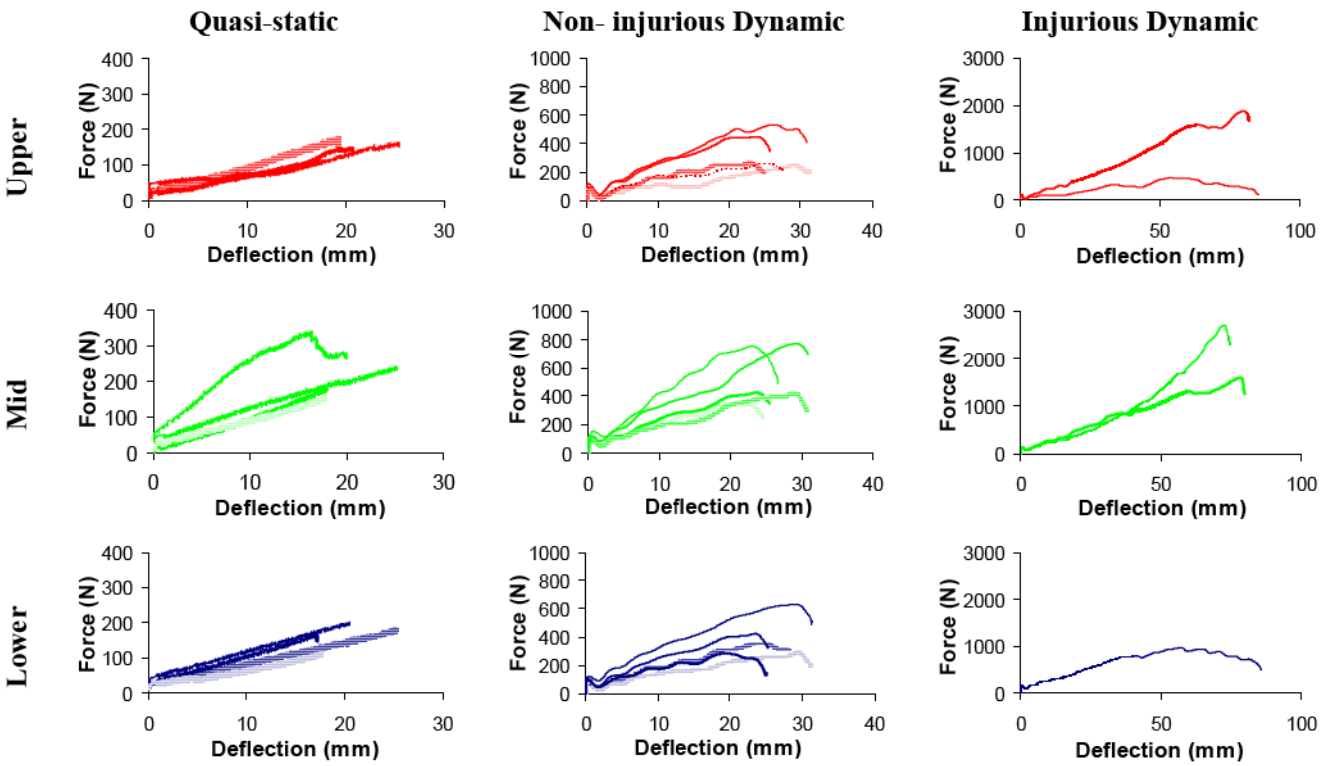

Figure 8. Force-deflection curves grouped by loading site and test type.

Effects of Indentor Orientation and Size: Figures 9 and 10 plot the force-deflection effects relative to variation in indentor orientation and size. All tests involved dynamic loading of subject 1 to a non-injurious level.

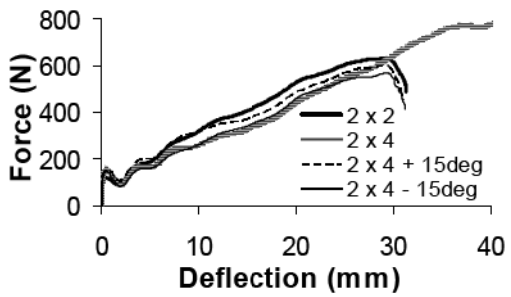

Figure 9. Force-deflection responses of subject 1 loaded at the lower site.

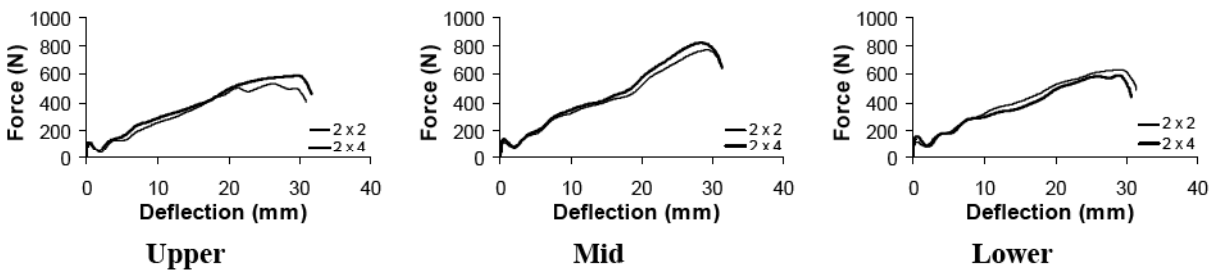

Figure 10. Subject 1 response to the 2x2" vs. 2x4" indentor.

Force-deflection results include a presentation of stiffness calculated using the load at 15 mm of indentor deflection divided by 15 mm. Figure 11 summarizes the indentor site stiffness of the subjects 2-5 for the quasi-static tests. Values ranged from 6.0 to 21.9 N/mm with an average value of 9.4 N/mm. Figure 12 presents the indentor site stiffness for the non-injurious dynamic tests. Values ranged from 6.4 N/mm to 37.6 N/mm with an average value of 18.7 N/mm, approximately twice the quasi-static test average.

The amount of variation in regional stiffness was subject dependent with subjects 2 and 5 showing the most variation. The mid site was the stiffest for both static and dynamic loading conditions for all subjects with the exception of Subject 3 dynamic test. The average of quasi-static and dynamic sternal stiffness was 18.1 N/mm. Although the average of quasi-static and dynamic stiffness of the lower site and the upper site were similar, 11.2 and 12.9 N/mm, respectively, the lower lateral site was stiffer than the upper site for three of the four subjects in the quasi-static tests and four of five subjects in the dynamic tests.

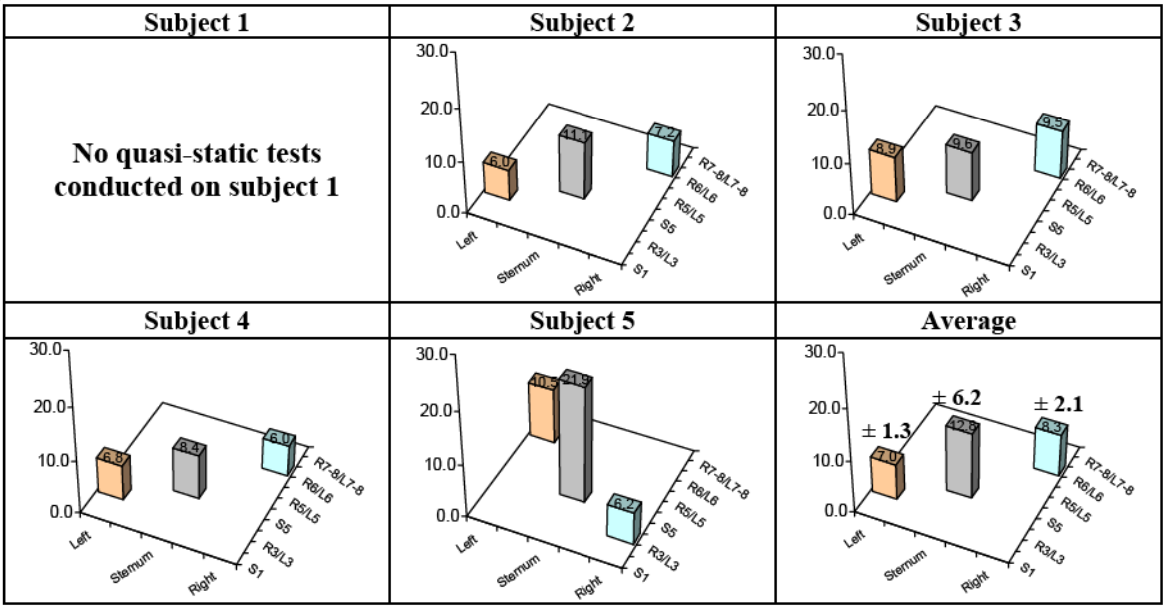

Figure 11. Regional subject stiffness resulting from quasi-static loading of subjects 2 – 5. No quasi-static tests were conducted on subject 1. Stiffness is reported in N/mm and was calculated by dividing the recorded indentor force at 15mm by the 15mm deflection.

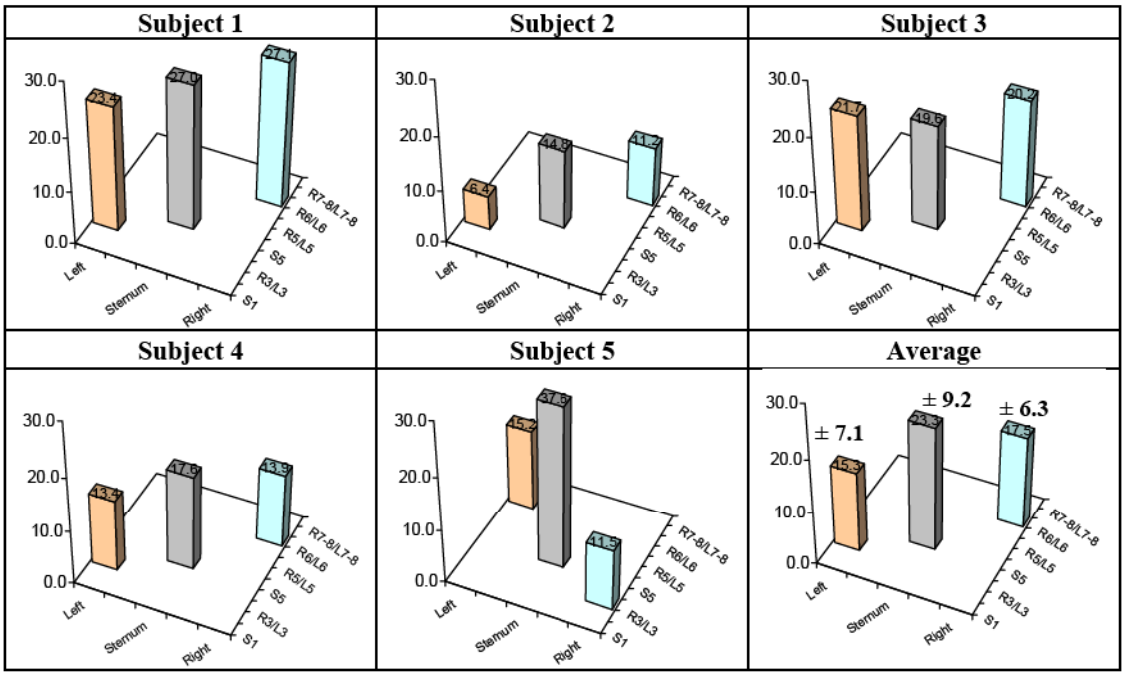

Figure 12. Regional subject stiffness resulting from non-injurious dynamic loading of subjects 1 – 5. Stiffness is reported in N/mm and was calculated by dividing the recorded indentor force at 15mm by the 15mm deflection.

COUPLING: The X-axis coupling patterns for the quasi-static and the dynamic tests were similar. Figure 13 presents the average coupling patterns for the non-injurious dynamic tests grouped by indentor site. The site deflection values were recorded at the time of peak indentor deflection. Appendix Figure A-1 presents coupling results for the tests to injury. The average response of subjects 2 and 3 are reported for the upper site loading condition and the average response of subjects 4 and 5 are reported for lower site loading. The response for subject 1 is presented for the lower site loading. The columns present coupling patterns when the indentor reached 20%, 30% of original chest depth and at failure. Appendix Figure A-2 illustrates the coupling effect on ribcage contours by using the H-model to animate the 3-D movement recorded by the Vicon cameras.

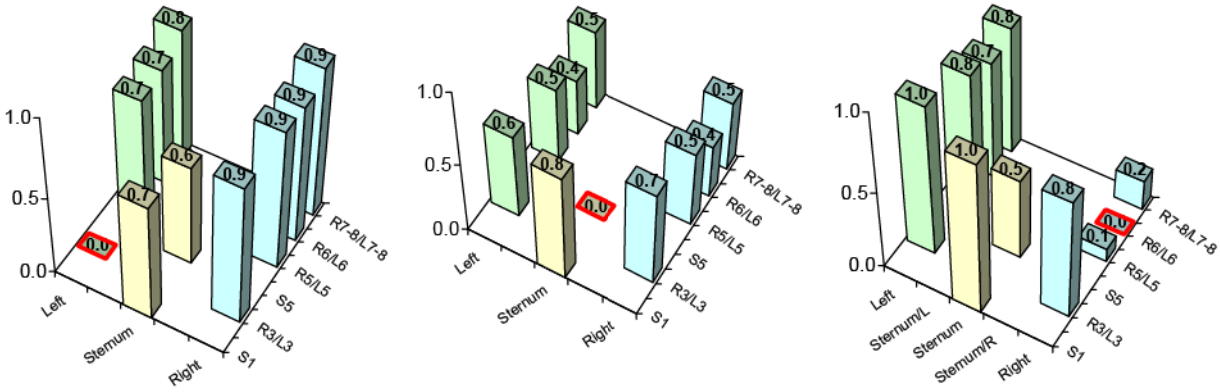

Upper **Mid** **Lower**

Figure 13. Coupling response averaged over all subjects for non-injurious dynamic tests by indentor site.

In addition to examining the deformation patterns for X-axis movement in the non-injurious dynamic tests, movement was recorded for the measurement sites in the Y-axis (positive to the subject's right) and Z-axis (positive toward the pelvis). Figure 14 presents the average deflection values for all three axes for the non-injurious dynamic tests. As indicated in the Methods section above, Y and Z-axis marker movements are affected by rotation of the rib or sternum.

FRACTURES: Autopsy identified a total of 61 fractures for the five subjects (Table 6). Most (25) were bi-cortical non-displaced fractures that involved disruption of both the outer and inner surfaces of the rib. There were 12 mono-cortical fractures in which either the outer or inner rib surface was disrupted. There were only four bi-cortical displaced fractures that involved a complete separation of the rib. There were 10 cartilage fractures and 10 "Other" fractures that includes disruption of the sterno-costal joint and incomplete rib fractures in which there is no cortical disruption but damage internal to the rib.

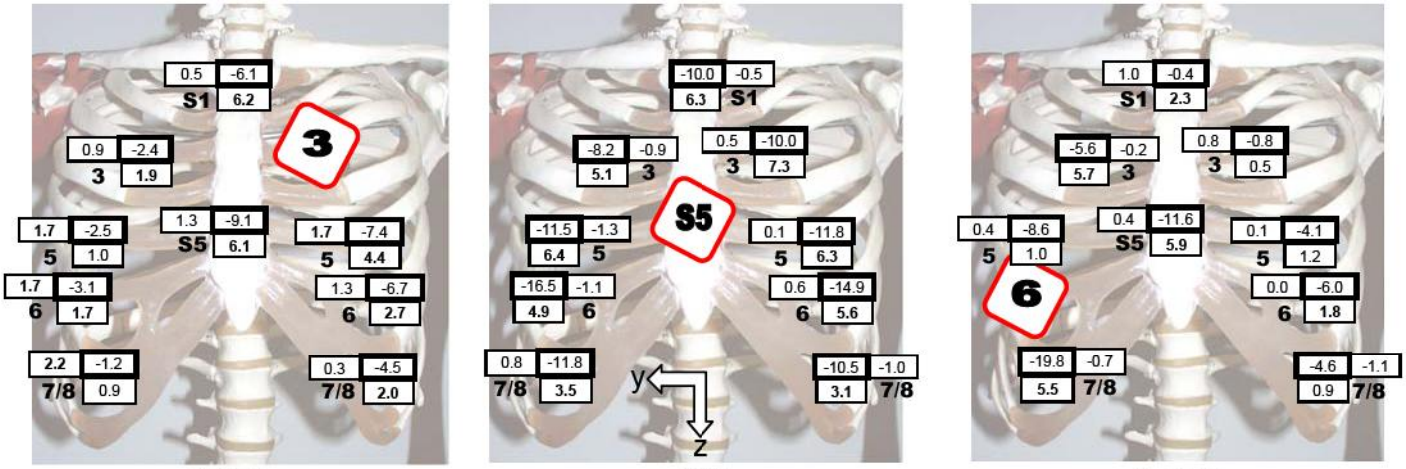

Upper Mid Lower

Figure 14. Average patterns of lateral and vertical ribcage motion for the non-injurious dynamic tests at peak indentor travel. The bold outline box indicates the location of the measurement site and contains the X-axis value. Negative X values indicates movement toward the spine. The lateral box indicates Y movement, positive to the subject's right. The box below the bold outline box indicates Z-axis movement, positive towards the pelvis. Rotation may contribute as much as 1.6 mm to apparent + Y and + Z site translation and up to -0.31 mm to apparent – Y and – Z site translation (see the Method section). Y and Z-axis values greater than these rotational bounds are shown in bold print.

Table 6. Fracture Summary

Subject	1	2	3	4	5	Total
Fracture Type						
Cartilage	4	1	1	2	2	10
Mono-cortical		3		9		12
Bi-coritcal Non-Displaced	11	4			10	25
Bi-coritcal Displaced		2	2			4
Other			1	6	3	10
Total	15	10	4	17	15	61

DISCUSSION

This study provides new information regarding the regional response of human cadavers subjected to anterior loading. Force-deflection, coupling, and the effects of rib fractures on response were the primary topics investigated.

FORCE-DEFLECTION: The study methodology, that involved loading each subject two to three times per site, risked changing the ribcage characteristics by each successive loading either by fracture or by permanent soft or hard tissue deformation. Over plots of the non-injurious dynamic tests with the dynamic failure tests suggest no change in response for subjects 2, 3, and 4. Subjects 1 and 5, those with the most calcified ribcages, appeared to be softer in the final injurious test (see Figure 15).

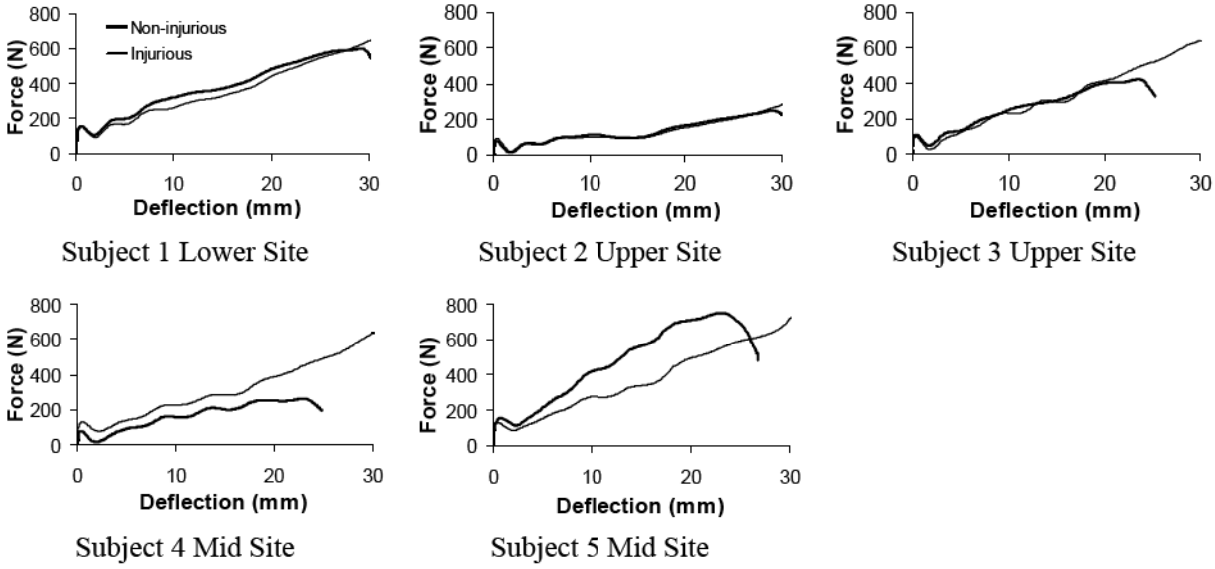

Figure 15. Force-deflection of the non-injurious dyanamic tests overplotted with the initial segment of the test that deformed the ribcage to an injurious level.

The quasi-static test force-deflection curves were generally linear over the 18-25 mm range of deflection suggesting an unvarying spring constant, a finding also reported by Eckert et al. (2000). The sole exception to this pattern was recorded for the subject 5 sternal loading during which the indentor rotated with respect to the ribcage. This resulted in a sudden unloading of the indentor at 16 mm (Figure 8). The dynamic test force-deflection curves exhibited an initial peak due to the inertial force needed to accelerate the anterior ribcage, a ramp to a peak value, and finally, a quick decline due to the rapid deceleration of the indentor and viscous relaxation (Figure 8, Non-injurious dynamic tests).

Viscous effects of the chest contributed significantly to thoracic stiffness. At 15 mm of deflection, the average dynamic test stiffness is twice that of the quasi-static test stiffness (Figures 11 and 12). This was expected given that, at 15 mm of deflection, the indentor was compressing the chest at approximately 1 m/s.

Indentor Size and Orientation Effects on Force-Deflection: The test conditions, varied for a single subject (1) in order to explore the effects of indentor size and orientation on the force-deflection response, produced similar results (Figures 9 and 10). The finding that a doubling in size of the indentor loading area from 26 to 52 cm^2 does not substantially affect force-deflection response suggests that the ribcage in the area of the indentor sites is locally coupled. This finding is supported by similar force-deflection responses recorded in a previous study in which the sternum was loaded by a 15 cm diameter, 177 cm^2 circular indentor (Kent et al., 2003c). Because the non-pivoting horizontal indentor face was not allowed to conform to the pretest sternal angle, the contact area size and geometry changed as the indentor compressed the thorax.

Note however that large indentors that span multiple areas of the anterior ribcage have been found to produce a stiffer response (Kent et al., 2003c). The insensitivity to indentor orientation, tested only at the lower site, also suggests local coupling and insensitivity to indentor rotation that may have occurred during loading.

RIB FRACTURE EFFECTS ON FORCE-DEFLECTION RESPONSE: Rib fractures have been shown to compromise the ability of the ribcage to bear load. Viano et al. (1978) found rib cage stability compromised at 32 percent chest deflection due to numerous rib fractures. However, others report that rib fractures have little or no effect on the force-deflection response. Kent et al. (2004) found that isolated rib fractures did not affect cadaver thoracic response in tests involving 1.0 m/s loading with various indentors. Another study in which the anterior thorax was loaded with a diagonal belt found that 35% compression and 12 to 20 rib fractures did not substantially affect the resultant reaction load (Duma et al., 2005).

The results of this study suggest that the occurrence of rib fractures does not necessarily reduce the ability of the chest to resist anterior loading. Figure 16 illustrates the variability of rib fracture effect. The number and type of fractures were similar for both subject 5 and subject 1. Except for a minor

spike at about 30 mm and a small dip at 60 mm, the subject 5 force-deflection curve exhibits a consistent rise. The subject 1 curve is similarly feature-free until about 40 mm. A series of spikes and decreasing slope begin at 55 mm suggesting that the ribcage is locally compromised by a series of fractures. Note, however, that the difference in loading sites likely contributed to the differences in the curves. The response of the mid site, supported by a greater number of redundant load paths, is less sensitive to multiple fractures.

Subject 4 sustained two more fractures than subject 5 but the force-deflection curve progressively increases suggesting that the ribcage became stiffer with increasing deflection (Figure 16). In this case, the type of fracture appears to be the reason for the difference in response. Subject 4 had no bicortical fractures while subject 5 had 10. The lack of bicortical fractures involving both the ventral and dorsal rib surfaces is consistent with the autopsy finding that the ribs were more pliable and the cartilage much less calcified than for subject 5. Apparently, subject 4's ribcage was less compromised by monocortical, cartilage, and other fracture types.

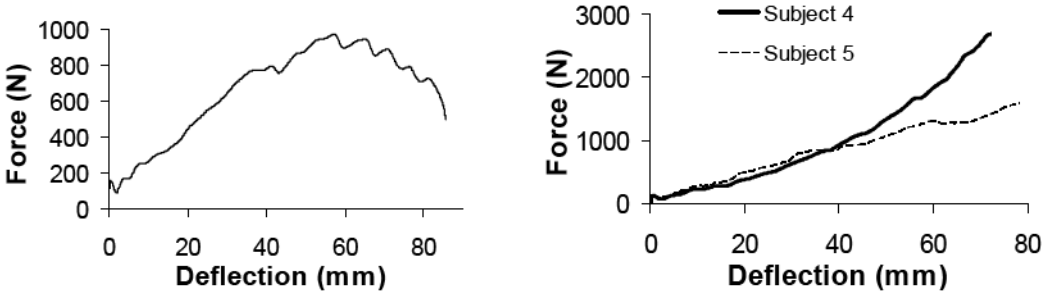

Subject	1	4	5
Site	Lower	Mid	
Total Fractures	15	17	15
Bicortical Fractures	11	0	10

Figure 16. Force-deflection response for subjects 1, 4 and 5 loaded.

Although the low number of subjects precludes definitive findings, the results indicate that subject age was related to the amount of ribcage calcification and the number of bicortical fractures, an indicator of more extensive ribcage structural compromise. The three older subjects, 67, 72, and 75 years at death, averaged 9 bicortical fractures compared to an average of 1 for each of the younger subjects with pliable cartilage, age 48 and 52 years at time of death. Ribcage calcification and fragility as a function of age has been well documented (Fayon et al., 1975, Kallieris, 2000, Kent et al., 2003a).

RIB FRACTURE PATTERNS: Rib fractures were observed to occur near the indentor and bilateral of the indentor site (Figure 17). All of the fractures for subject 3 and half for subject 2 were located under or near the indentor site. This was due to the indentor plate pushing through the ribcage during the failure tests creating the only displaced fractures observed in the test series. Qualitative assessment of rib strength, the amount of osteopenia evident on the CT images, varied considerably for the two subjects - "moderate-to-severe" for subject 2 and "mild" for subject 3 (Table 2). Further study with additional subjects is required to determine if the structural configuration of the upper lateral region of the ribcage predisposes it to failure from concentrated loading.

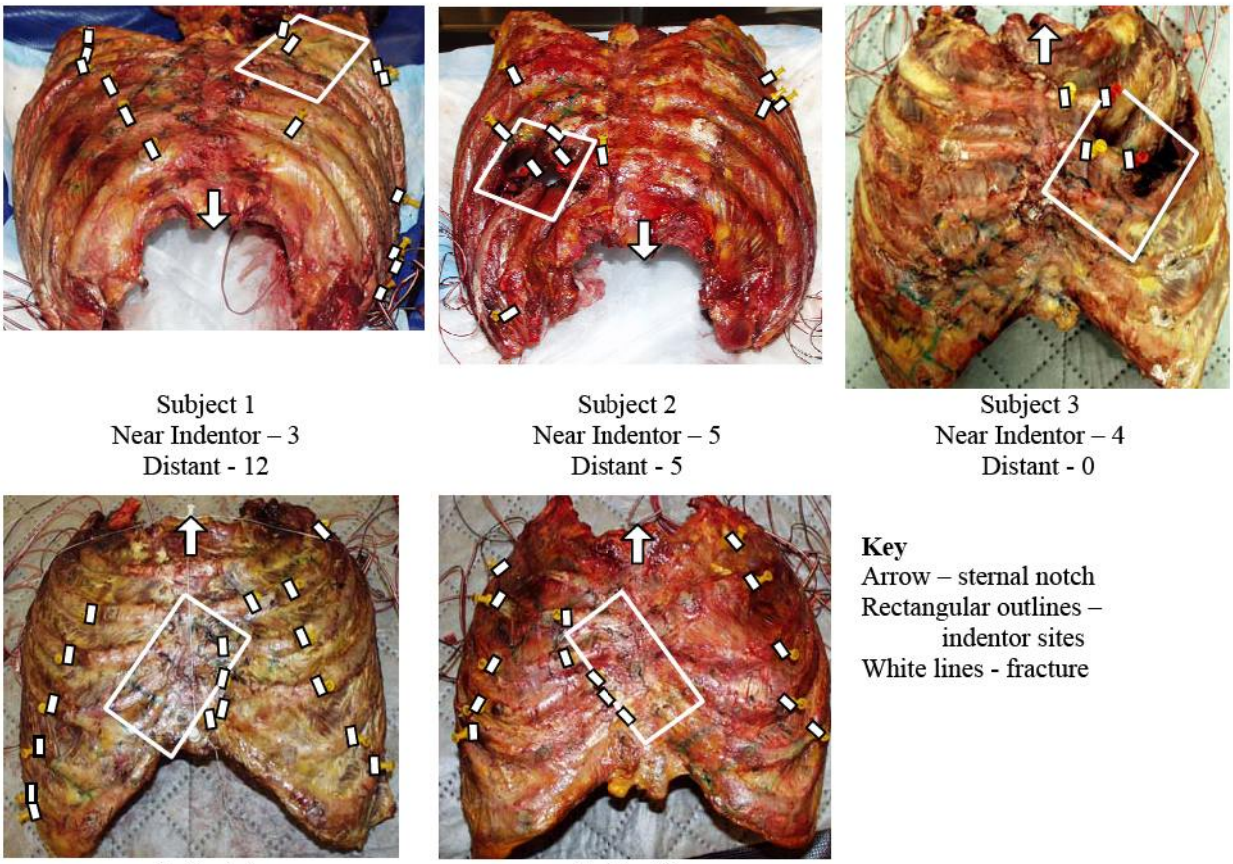

Figure 17. Rib fracture patterns including fracture distribution. The indentor pushed through the ribcage for subjects 2 and 3.

For the other tests in which the ribcage remained intact, at least twice as many fractures occurred lateral to the indentor site as near the indentor site. For subject 1, there was a fracture line to the left of the indentor site that coincided with four of the five fractures occurring at the costo-chondral junction. Six fractures were located far laterally to the right of the indentor site, two occurred at the strain gage location. For subject 4, the fractures occurred primarily along three lines that defined the left border of the indentor (4) and the left and right costo-chondral boundaries (7). Subject 5 exhibited a similar distribution though fewer costo-chondral fractures.

Costo-chondral junction fractures are common in cadaver frontal sled tests that use a diagonal shoulder belt restraint (Kent et al., 2003b, Petitjean et al., 2002). Belt loading often results in fractures along the belt or belt edge (Patrick and Andersson, 1974, Cesari and Bouquet, 1990, Kallieris et al., 1980, and Crandall et al., 1996) apparently due to local stress concentration. Note that the subjects in this study may have experienced more of these loading site fractures due to the removal of the overlying soft tissue that may help distribute the applied load.

Fractures that occur away from the loading site, especially those on the lateral ribcage, are apparently due to overall ribcage deformation with the primary mode being the anterior displacement (Berthet and Vezin, 2006).

REGIONAL STIFFNESS: Identification of the mid site as the stiffest region was not unexpected (Figures 11 and 12). However, the observation that the lower loading site proved as stiff, or slightly stiffer, than the upper loading site was surprising. We expected that the upper site being closer to the sternal midline would have resulted in greater stiffness. In comparison to the sixth rib, the third rib also has a shorter cartilaginous section anchoring it to the sternum (Figure 18).

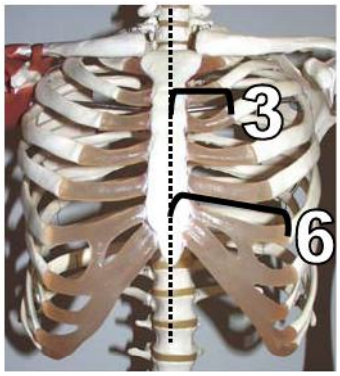

Figure 18. Location of third rib (upper) and sixth rib (lower) indentor loading targets.

Subject 3 recorded the least variation in stiffness for the three loading sites and subject 5 the greatest (Figures 11 and 12). Explanations for this finding may reflect differences in the ribcage structural properties. Subject 5, 72 years at death, had a stiffer, more calcified ribcage than subject 3, a 48 year old with more pliable cartilage.

COUPLING: Because the coupling patterns in the quasi-static and the dynamic tests produced similar qualitative results, the following discussion is based on the non-injurious dynamic test results which included all five subjects.

Subject Variation: Loading at the three sites produced a similar X-axis deflection coupling pattern for each subject although there was subject-to-subject variation. Subjects 1 and 5 were most coupled when loaded at the mid site.

Coupling Patterns: Loading the upper site results in moderate deflection in the adjacent (S1) and (S5) sites as well as in fifth rib and sixth rib sites on the side of the loading (Figure 13).

Loading (L6) produces substantial deflection in the adjacent rib 5 and 7-8 sites as well as moderate deflection at (S5). For subjects 1 and 5, the lower sternum seems to be a pathway for modest deflection of the lower ribcage sites on the side opposite the loading location. The average coupling reflects this as a moderate deflection of (R6) (Figures 13 and 19). Loading the mid site produces general deflection bilaterally with the greatest deformation occurring at (R6) and the least at (L3).

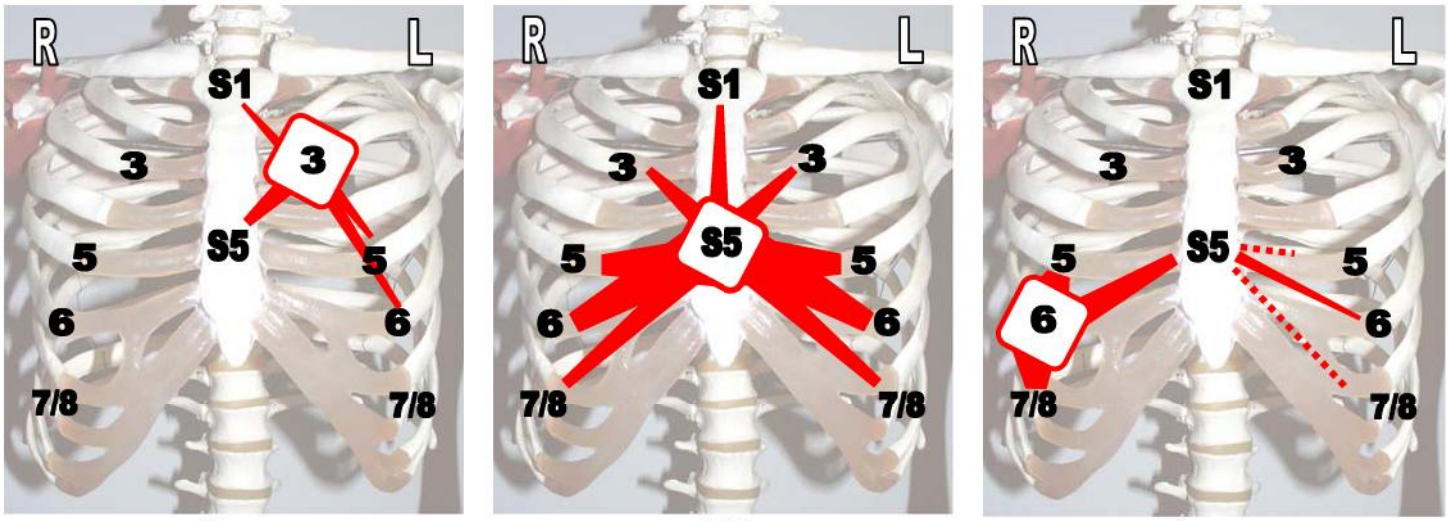

Upper Mid Lower

Figure 19. Coupling patterns by loading sites using average data from the non-injurious dynamic tests. The width of the radiating lines indicates the amount of X-axis deflection, a measure of coupling, observed between the indentor site and the other sites. The dashed lines indicate a coupling trend not reflected in the average.

Except for the upper loading case, (S1) deflected the least. The observation that the upper sternum was well supported is consistent with the stiffness results reported by Schneider et al. (1992b). The

upper sternal site was found to be the stiffest site, 18 percent stiffer than the mid sternum, and 44 percent stiffer than the lower sternal sites.

COUPLING PATTERNS AT GREATER INDENTOR DEFLECTION: The tests to injury, that involved indentor deflection of approximately 80 mm, produced coupling patterns (Appendix Figure A-1) similar to those recorded in the non-injurious tests in which the peak indentor deflection was approximately 30 mm. There were minor variations in coupling pattern for the upper and mid site loading. In the upper site case, there appeared to be a modest unloading of ribs 5 and 6 on the side loaded between the 30 percent and the injurious loading level in response to the indentor causing local failure. The overall similarity in coupling patterns over a wide range of indentor deflection levels suggests that coupling is a stable characteristic of the ribcage structure and is largely unaffected by multiple rib fractures.

PATTERNS OF LATERAL AND VERTICAL RIBCAGE MOTION: In all but two cases, the magnitude of X-axis movement exceeded that of Y and Z-axis movement, often by a wide margin, a finding consistent with that reported for a study that involved static loading of cadaver ribcages with a simulated diagonal belt (Ali et al., 2005) (Figure 14).

Given the inferior slope of the ribs, the movement of the monitored sites was toward the pelvis (+Z) for all loading conditions. Z-axis movement was most pronounced for the sternum, adjacent to the loading site in the upper loading condition. The magnitude of the (S1) Z-axis value was greater than that of the X-axis deflection. Lower site loading also produced the greatest Z-axis movement in sites near the loading location. The mid loading condition produced generalized Z-axis movement that, for five of nine sites, was at least half of the X-axis value. Movement of the anterior ribcage toward the pelvis in response to normal loading has been reported for a hub-anterior thorax impact test (Schneider et al., 1992a).

There was relatively little lateral (Y-axis) movement for all of the loading conditions. All sites moved to the right when the upper left was loaded. Y-axis movement for the mid loading condition suggests that the both sides of the ribcage moved toward the centerline in response to sternal movement toward the spine generating a local concavity of the anterior ribcage. Lower site loading produced no discernable Y-axis movement pattern.

As indicated in the Methods section, caution should be exercised when interpreting these results. Although the Vicon camera system tracked the markers with an accuracy of $\pm$ 0.3 mm, rib and sternal rotation may account for as much as 1.6 mm of apparent positive Y and Z movement and -0.31mm of negative Y and Z movement.

CAVANAUGH TEST COMPARISON: The method for the tests reported for this study (Table 7) approximated that of the Cavanaugh tests of the cadavers conducted at Wayne State University. However, differences in methodology (Table 7, Figure 20) should be considered when comparing results (Figure 21).

Table 7. Differences in Test Methodology Between Cavanaugh and UVA Tests

	Cavanaugh	**UVA**
Subject preparation	Denuded	Denuded anteriorly and laterally
Subject support	Spine and ribs supported.	Spine and ribs supported. Spine screwed to support.
Indentor	62 x 113 mm (2x4")	62 x 113 mm (2x4") and 62 x 62 mm (2x2") Center of rotation of indentor head nearer to contact surface.
Indentor velocity	Quasi-static	Quasi-static and dynamic (1.0m/s)
Indentor sites	Sternum: at rib 2 and at rib 6 Lateral: Right side, 75 mm from centerline ribs 2, 5, 8	Sternum: at rib 5 Lateral: Left[A] side rib 3 at costo-chondral (CC) junction, right side at rib 6 CC.
Deflection measurement	8 sites [B] (indentor sites) reported	10 sites [B]: 3 indentor sites + Sternum at rib 1 Right side rib 3 at CC Bilateral rib 5 at CC Left side rib 6 at CC Bilateral rib7-8 junction

Notes
A - Subject 5 reversed left and right lateral indentor sites.
B - Often some of the measurement sites unavailable because of interference with the indentor.

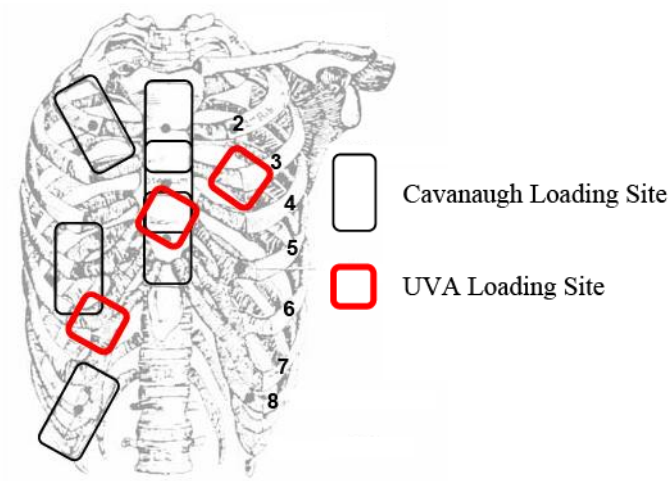

Figure 20. Differences in Cavanaugh and UVA loading sites.

The average upper and sternal loading site stiffnesses were similar for the Cavanaugh and UVA studies (Figure 21). Cavanaugh also found that the upper and mid lateral sites were similarly stiff, a three-subject average of 6.63 N/mm for the second rib and 6.33 N/mm for the fifth rib. The stiffnesses of the mid lateral Cavanaugh site and the UVA lower site were also similar, apparently due to similar locations on the ribcage (Figure 21).

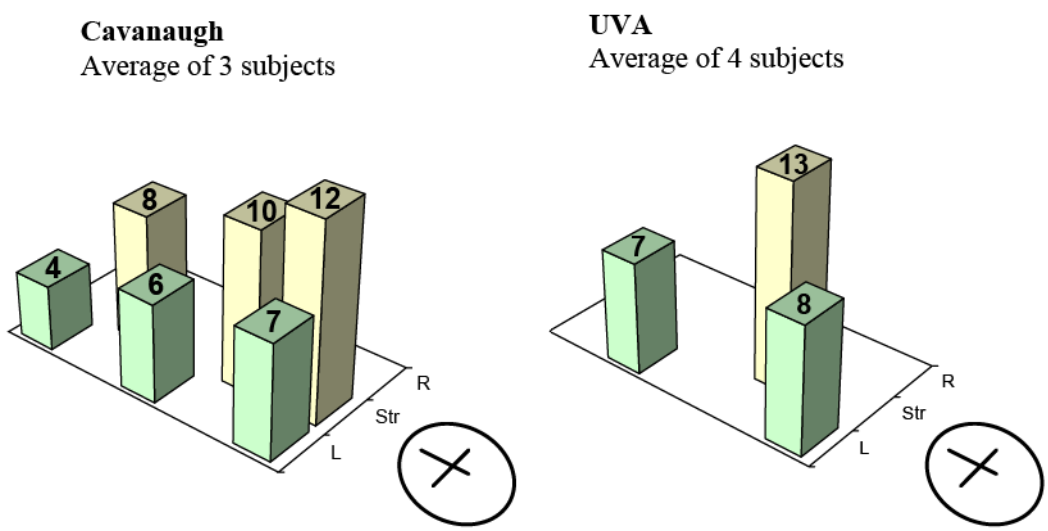

Figure 21. Regional stiffness (N/mm) comparison between Cavanaugh and UVA quasi-static thoracic loading tests. L/R symmetry assumed.

Table 8. UVA Test Conditions vs. Actual Crash Environment

Crash	UVA Bench-Top	Comment
Inertially loaded erect thorax translates and rotates until arrested by the shoulder belt.	Stationary thorax constrained by spinal fixation in supine position. Posterior ribcage motion is limited by rigid platen.	
Viscera translate forward inside thorax and loads the anterior ribcage.	Constant velocity tests have only a minor inertial contribution from the anterior ribcage.	
Continuous loading from shoulder to lower border of ribcage by shoulder belt and air bag.	Serial segmental loading by rigid indentor constraint to move only in one axis. The effect of shoulder load sharing not investigated.	Bench top test condition isolates loading to a small region while modern restraints distribute the load more widely.
Subject thorax skin intact.	Skin and other soft tissues removed from anterior and lateral thorax.	Removing all of the skin and soft tissues reduces ribcage stiffness 40% in an anterior hub loading bench top test environment (Kent et al., 2005). The effect on coupling is unknown.

STUDY LIMITATIONS AND RECOMMENDATIONS FOR FURTHER INVESTIGATION

Although the study was successful in providing useful information, the results should be used with the understanding that there were limitations due to study design and execution. The primary limitation involves subject position and fixation. The bench-top test fixture, while an excellent test environment in which to make measurements, deviates from the loading environment experienced by a vehicle occupant in a crash (Kent et al., 2004) (Table 8) .

Other study limitations included few subjects and subject-to-subject variation, which precluded statistically significant findings for the observed differences in regional stiffness (single-tailed heteroscedastic t-test, $p < 0.05$). While multiple tests per subject improved the amount of information for the non-injurious loading tests, only one injurious loading test per subject was conducted resulting in only one or two tests at the three loading sites. The indentor pushed through at the upper site for two of the five subjects. Testing with additional subjects is required to determine if this region of the ribcage is particularly susceptible to catastrophic failure and to establish injury thresholds for all regions of the anterior ribcage.

The non-injurious tests which involved four to five subjects loaded at the same locations produced considerable variability. For example, the force at 15 mm of deflection ranged from 200 to 570 N.

The method used to track the 3-D motion of the rib sites was inexact due to the lack of rib (or sternal) rotation information provided by a single marker. Motion tracking systems require a minimum of three markers per site to produce rigid body 3-D translation and rotation data necessary to determine how the rib moves (Eckert et al., 2000).

IMPLICATIONS FOR SURROGATE RIBCAGE DESIGN

The findings of this and prior studies of cadavers (Schneider et al., 1989, 1992b), L'abbe et al., 1982, Kent et al., 2005) provide insight to the mechanisms governing ribcage response to anterior loading.

The force-deflection response to quasi-static loading is approximated by that of a spring with an unchanging spring constant. Dynamic loading, at a rate similar to that of contemporary belt restraints in a 48 km/h frontal crash, produced a response complicated by inertial and viscous components that were less prominent than that reported for the higher speed Kroell hub impact tests (Kroell, 1994).

The insensitivity to indentor size and orientation suggests a local plate motion indicating substantial coupling provided through the sternum and intercostal soft tissue. Redundant coupling of the ribs may

also help explain why rib fractures do not have a more noticeable effect on the force-deflection response. However, the results suggest that the effect of rib fractures cannot be ignored, especially for loading of sites such as the lower lateral ribcage that have less redundant support than areas such as the central sternum. The finding that the type and not just the number of rib fractures should be considered when evaluating ribcage structural integrity is also useful information that can be used to assess the utility of cadaver test data. Moreover, the finding of this and other studies (Kent et al., 2004, Duma et al., 2005) indicating that isolated fractures have little or no effect on the force-deflection response, indicates that cadavers who have sustained fractures during the testing may nevertheless be useful in establishing surrogate response performance criteria.

The similarity of coupling patterns for indentor loading through the failure level provides evidence that multiple rib fractures have a minor effect on structural response and that coupling is relatively constant over a wide range of anterior loading levels. If confirmed by testing with a larger sample size, this finding suggests that a ribcage surrogate may not have to model fracture and coupling that varies with deflection.

SUMMARY AND CONCLUSIONS

This study provides data regarding the regional response of the human cadaver thorax when subjected to anterior loading. Force-deflection, mechanical coupling, and the effects of rib fractures on response were explored.

1. The quasi-static test force-deflection curves were generally linear.
2. At 15 mm of deflection, the average dynamic test stiffness is twice as high as the quasi-static test stiffness due to the viscous reaction force not present in the quasi-static loading condition.
3. The results of this study suggest that the occurrence of rib fractures does not necessarily reduce the ability of the chest to resist anterior loading. The effects of rib fracture are most evident when loading the lower rib cage and when there are many bicortical fractures. Little effect was seen for sternal loading and for multiple non-bicortical fractures.
4. Bicortical fractures were associated with subjects whose ribcage cartilage was more calcified, a condition more common for the older subjects.
5. Many of the rib fractures occurred at the costachondral junction.
6. The sternal site was stiffest. The average stiffness of the upper and lower sites was about the same but the lower site was somewhat stiffer for most of the subjects.
7. The average upper and mid loading site stiffnesses were similar for the Cavanaugh and UVA studies. Differences in stiffness values for the mid to lower ribcage site may be explained by differences in test conditions.
8. The coupling patterns were similar for the quasi-static and the dynamic tests.
9. Loading at the three sites produced a similar X-axis deflection coupling pattern for each subject although there was subject-to-subject variation.
10. Coupling patterns were similar at increasing indentor deflection level.
11. In general, coupling patterns found in this study were similar to those found by Cavanaugh despite differences in test conditions.
12. In most cases, the deflection toward the spine was greater than the lateral and inferior movement at any measurement site. At any site, only positive Z-axis motion (toward the pelvis) was observed.

Although the study was successful in providing useful information, limitations of the study including a test environment that is quite different from that of a frontal crash and a small number of subjects should be considered when using study results and / or methods to develop surrogates.

Further study of cadaver and surrogate thoracic response, both at a component level on the bench top and at a systems level in a simulated crash, is needed to advance the development of surrogates better able to respond biofidelically to contemporary restraint loading.

ACKNOWLEDGEMENTS

NHTSA's Research and Development Program provided both technical direction and financial support. Vicon Peak provided the Vicon camera system used for 3-D tracking of points on the anterior ribcage. Tim Gillispie helped prepare the paper for publication.

REFERENCES

Ali, T, Kent, R, Murakami, D, Kobayaashi, S. (2005) Tracking Rib Deformation Under Anterior Loads Using Computed Tomography Imaging. SAE Transactions: Journal of Passenger Cars, 114(6): Based on SAE Paper 2005-01-0299.

Backaitis, S ed. Biomechanics of Impact Injury and Injury Tolerances of the Thorax-Shoulder Complex. Society of Automotive Engineers Publication PT-45. 1994.

Berthet, F, Vezin, P. APROSYS SP5 Review of the Thorax Injury Criteria Report D514A – Part A, AP-SP51-0038-B. October 2006.

Cavanaugh J, Jespen K, King A. (1988) Quasi-static frontal loading to the thorax of cadavers and Hybrid III dummy. Proceedings of the 16th International Workshop on Human Subjects for Biomechanical Research, Atlanta, GA. pp 3-18.

Cesari, D.; Bouquet, R. 1990. Behavior of human surrogates thorax under belt loading. Stapp Car Crash Conference. Thirty-Fourth. Proceedings. SAE, p. 73-81. Report No. SAE 902310.

Crandall, JR, Bass, C, Pilkey, W, Morgan, R, Eppinger, R, Miller, H, Sikorski, J. (1996) An Evaluation of Thoracic Response and Injury with Belt, Airbag, and Constant Force Retractor Restraints', NATO Conference on Crashworthiness in Transportation Systems: Structural Impact and Occupant Protection, Troia, Portugal.

Crandall, JR, Bass, C, Pilkey, W, Morgan, R, Eppinger, R, Miller, H, Sikorski, J. (1997) Thoracic Response and Injury with Belt, Driver Side Airbag, and Constant Force Retractor Restraints. International Journal of Crashworthiness, 2(1): 119-132.

Duma, S.; Stitzel, J.; Kemper, A.; McNally, C.; Kennedy, E.; Matsuoka, F. 2005. Acquiring non-censored rib fracture data during dynamic belt loading tests on the human cadaver thorax. Report No. 05-0360-O. Proceedings of the 19th International Technical Conference on the Enhanced Safety of Vehicles, 2005.

Eckert, M.; Fayet, M.; Cheze, L.; Bouquet, R.; Voiglio, E.; Verriest, J. P. 2000. Costovertebral joint behavior during frontal loading of the thoracic cage. International IRCOBI Conference on the Biomechanics of Impacts. Montpellier (France), p. 195-206.

Eppinger, R. H.; Morgan, R. M.; Marcus, J. H. (1984) Side impact data analysis. National Highway Traffic Safety Administration, Washington, D.C. 7 p. Proceedings of the 9th International Technical Conference on Experimental Safety Vehicles. 244-250.

Fayon, A.; Tarriere, C.; Walfisch, G.; Got, C.; Patel, A. 1975. Thorax of 3-point belt wearers during a crash (experiments with cadavers) Stapp Car Crash Conference. Nineteenth. Proceedings. Warrendale, Society of Automotive Engineers, 1975, p. 195-223. Report No. SAE 751148.

Handbook of Numerical Analysis, Volume XII: Computational Models for the Human Body – Human Models for Crash and Impact Simulation, pp 297-361, Elsevier, 2004

Kallieris D (2000) The Biomechanics of Frontal and Lateral Collision, in Human Biomechanics and Injury Prevention, ed. By J. Kajzer, E. Tanaka, H. Yamada, Springer Tokyo, p. 41-50.

Kallieris, D.; Barz, J.; Schmidt, G. 1980. Influence of the belt width in regard to the injury severity and injury pattern at the thorax. Reich, H., ed. International Association for Accident and Traffic Medicine. Eighth International Conference. Proceedings. Aarhus, Danish Society for Traffic Medicine, p. 120-126.

Kent, R, Lessley, D, Sherwood, C. (2004) Thoracic response to Dynamic, Non-Impact Loading from a Hub, Distributed Belt, Diagonal Belt, and Double Diagonal Belts. Stapp Car Crash Journal, 48:495-519.

Kent, R, Murakami, D, Kobayashi, S. (2005) Frontal thoracic response to dynamic loading: the role of superficial tissues, viscera, and the rib cage. International IRCOBI Conference on the Biomechanics of Impacts. Prague (Czech Republic), p. 355-365.

Kent, R, Patrie, J, Poteau, F, Matsuoka, F, Mullen, C. (2003a) Development of an age-dependent thoracic injury criterion for frontal impact restraint loading. Paper 72, Proceedings of the 18th International Technical Conference on the Enhanced Safety of Vehicles.

Kent, R, Shaw, G, Lessley, D, Crandall, JR, Kallieris, D, Svensson, M. (2003b) Comparison of belted Hybrid III, THOR, and cadaver thoracic responses in oblique frontal and full frontal sled tests. Paper 2003-01-0160, Society of Automotive Engineers.

Kent, R, Sherwood, C, Lessley, D, Overby, B, Matsuoka, F. (2003c) Age-related changes in the effective stiffness of the human thorax using four loading conditions. IRCOBI Conference on the Biomechanics of Impact.

Kroell, C Thoracic response to blunt frontal loading in The Human Thorax – Anatomy, Injury, and Biomechanics, Society of Automotive Engineers publication P-67, pp 49-77. Reprinted in Biomechanics of Impact Injury and Injury Tolerances of the Thorax-Shoulder Complex, Backaitis (ed.), Society of Automotive Engineers 1994 publication PT-45, pp 51-79.

Kuppa, S. M.; Eppinger, R. H. 1998. Development of an improved thoracic injury criterion. Stapp car crash conference. Forty-second. Proceedings. SAE, 1998, p. 139-153. Report No. SAE 983153.

L'Abbe, R. J.; Dainty, D. A.; Newman, J. A. 1982. An experimental analysis of thoracic deflection response to belt loading. International IRCOBI Conference on the Biomechanics of Impacts. VIIth. Proceedings. Bron, IRCOBI, 1982, p. 184-194.

Mulligan, G.W.N., Pizey, G., Lane, D., Andersson, L., English, C., Kohut, C. (1994) An introduction to the understanding of blunt chest trauma. In Biomechanics of Impact Injury and Injury Tolerances of the Thorax-Shoulder Complex, ed. Backaitis, S., pp. 11-36, Society of Automotive Engineers Publication PT-45.

Patrick, L. M.; Andersson, A. 1974. Three-point harness accident and laboratory data comparison. Stapp Car Crash Conference. Eighteenth. Proceedings. Society of Automotive Engineers, 1974, p. 201-282. Report No. SAE 741181.

Petitjean, A.; Lebarbe, M.; Potier, P.; Trosseille, X.; Lassau, J.-P. 2002. Laboratory reconstructions of real world frontal crash configurations using the Hybrid III and THOR dummies and PMHS. Stapp Car Crash Journal, Vol. 46, p. 27-54. Report No. SAE 2002-22-0002.

Schneider, L. W.; Haffner, M. P.; Eppinger, R. H.; Salloum, M. J.; Beebe, M. S.; Rouhana, S. W.; King, A. I.; Hardy, W. H.; Neathery, R. F. 1992a. Development of an advanced ATD thorax system for improved injury assessment in frontal crash environments. Stapp Car Crash Conference. Thirty-sixth. Proceedings. SAE, p. 129-155. Report No. SAE 922520.

Schneider L, King A, Beebe M (1989) Design Requirements and Specifications: Thorax-Abdomen Development Task. Interim Report: Trauma Assessment Device Development Program. DOT HS 807 511. November 1989.

Schneider, L, Ricci, L, Salloum, M, Beebe, M, King, A, Rouhana, S, Neathery, R. (1992b) Design and Development of an Advanced ATD Thorax System for Frontal Crash Environments. Final Report Volume 1: Primary Concept Development. Trauma Assessment Device Development Program. DOT HS 808 138. University of Michigan Transportation Research Institute. June 1992.

Shaw, G, Lessley, D, Kent, R, Crandall, JR. (2005) Dummy Torso Response to Anterior Quasi-Static Loading. Paper 05-0371, Proceedings of the 19th International Technical Conference on the Enhanced Safety of Vehicles.

Shaw, G, Lessley, D, Bolton, J, Crandall, JR. (2004) Assessment of the THOR and Hybrid III Crash Dummies: Steering Wheel Rim Impacts to the Upper Abdomen. Paper 2004-01-0310, Society of Automotive Engineers.

Yoganandan, N.; Skrade, D.; Pintar, F. A.; Reinartz, J.; Sances, A., Jr. 1991. Thoracic deformation contours in a frontal impact. Stapp Car Crash Conference. Thirty-fifth. Proceedings. SAE, Nov 1991, p. 47-63. Report No. SAE 912891.

Viano, D. C.; Haut, R. C.; Golocovsky, M.; Absolon, K. 1978. Factors influencing biomechanical response and closed chest trauma in experimental thoracic impacts. Proceedings of the 22nd American Association for Automotive Medicine Conference and the International Association for Accident and Traffic Medicine, VII Conference. Proceedings. Volume 1, AAAM, 1978, p. 67-82.

APPENDIX

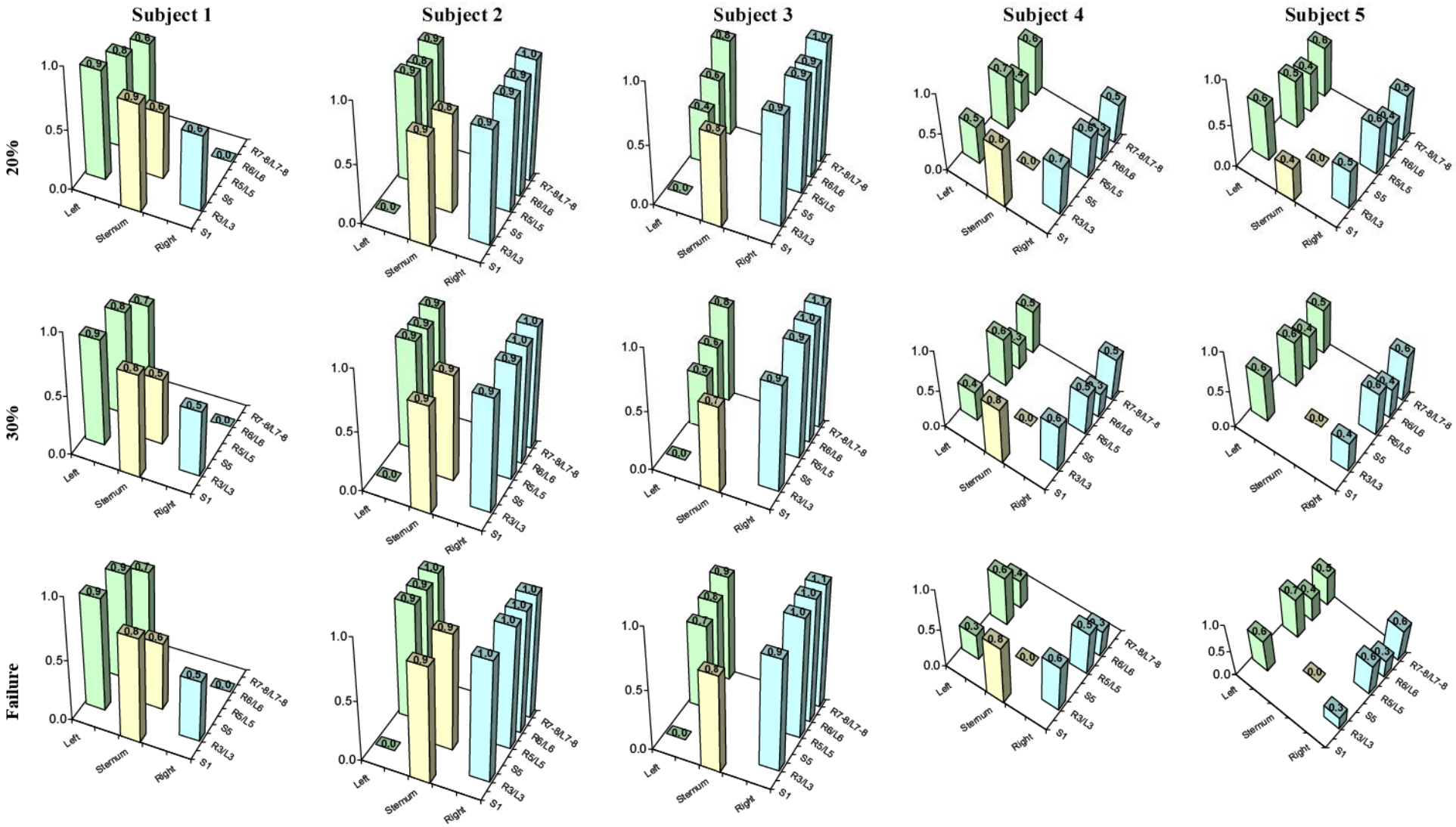

Figure A-1. Coupling results for the tests to injury. The upper and mid site results are the average of two subjects. The lower results are for a single subject. Coupling patterns are presented when the indentor reached 20, and 30 % of original chest depth and at failure.

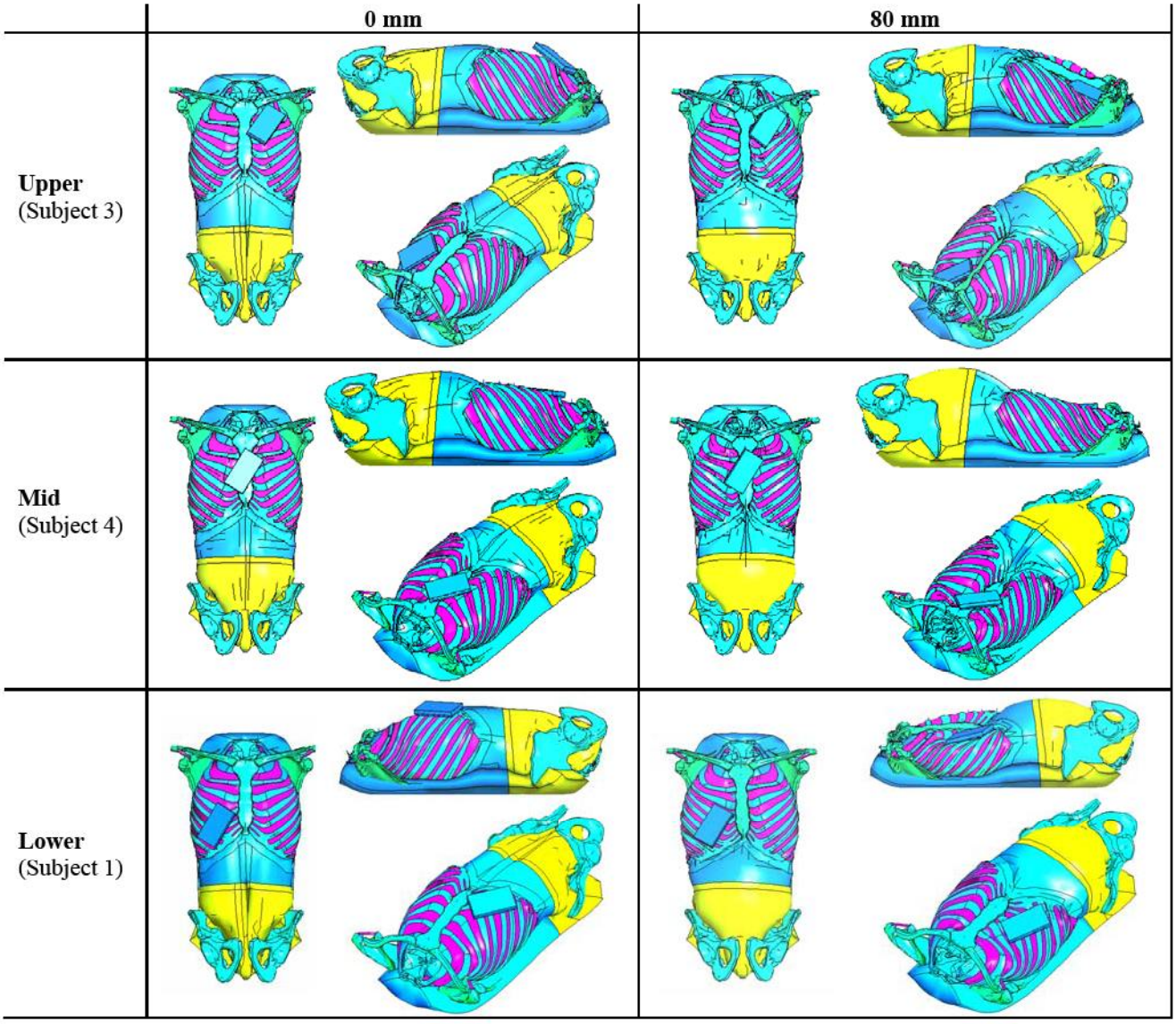

Figure A-2. Coupling results for the tests to injury. Thorax contours for subjects 1, 3 and 4 are presented for indentor travel of 0 mm and 80 mm.